JOURNAL OF MATERIALS SCIENCE 12 (1977) 141–152

The effect of microstructure and crystallinity on the tensile properties and fracture behaviour of injection-moulded polytetramethylene terephthalate

J. E. CALLEAR, J. B. SHORTALL
Department of Metallurgy and Materials Science, University of Liverpool, Liverpool, UK

The variation in morphology and crystallinity across injection-moulded ASTM bars of the semi-crystalline thermoplastic, polytetramethylene terephthalate (PTMT), has been characterized by optical microscopy and X-ray diffraction techniques and related to the initiation and mode of fracture of the material. Optical microscope observation of microtomed sections reveal a gradual variation of morphology from skin to core with changes in spherulite size and distribution together with flow patterns within the outer skin and core contributing to the overall complexity. An increase in crystallinity has been found to occur in the non-flow regions and the fracture behaviour and modes of deformation have been interpreted in terms of the band structure and related to the flow patterns. A modification of Tadmor's model is shown to adequately represent the mould-filling process.

1. Introduction

Polytetramethylene terephthalate (PTMT) also known as polybutylene terephthalate (PBT) is a thermoplastic designed primarily for the injection moulding of engineering parts. The mechanical properties of such a material are highly sensitive to morphological changes produced on moulding and are dependent upon the characteristic skin–core morphology [1–4] which is developed during moulding causing orientation of polymer chains with the possibility of built in stress distribution [5–7]. The moulded part can then be considered a composite resulting from recrystallization during the various stages of moulding in which a number of distinct crystalline zones have been shown to form [8, 9]. These zones have been identified as a highly oriented non-spherulite skin, a row or shear nucleated spherulitic intermediate layer and a spherulitic core [8]. Shear orientation predominates and the final orientation depends on the thermodynamic relaxation effects involved; the oriented molecules may relax as long as the melt is not frozen with a reduction in orientation [10]. Changes in microstructure in different regions of the moulded part have been shown to give a variation in mechanical properties within the moulding [3]. These microstructural changes along with accompanying changes in morphology would be expected to have a marked effect on crystallinity and fracture behaviour across the specimen, also, orientation and crystallinity will have an effect on such properties as ultimate tensile strength and elongation to failure [10]. Ballman and Toor [6] related observed birefringence to molecular orientation and postulated a mechanism for non-isothermal flow in which shear flow was the main source of orientation and molecular relaxation after cessation of flow was the process which reduced orientation.

The results of Menges and Wübken [5] are in qualitative agreement with those of Ballman and Toor [6], indicating a complex orientation distribution with one or more maxima, but they

attribute orientation not only to shear flow but also to the advancing shear front. A model which combines flow patterns with molecular theories and the heat transport problem and which predicts semi quantitatively the observed complex orientation pattern has been postulated by Tadmor [7]. This model implies that fluid particles which hit the cold wall will immediately solidify, freezing in the orientation induced by the elongational flow they have experienced. The magnitude of this orientation depends on the rate of elongation. The surface layer (skin) thus retains the maximum orientation induced in the front. Tadmor then includes the effects of the shear stress and shows that the shear rate is zero at the solid interface, goes through a maximum and drops to zero at the centre. The shear rate distribution, immediately prior to cessation of flow determines the initial shear oriented distribution. Upon cessation of flow relaxation of molecular orientation between the solidified skin layers begins. The time for relaxation is determined by the distance from the surface. Tadmor concludes that this fits semi-qualitatively the orientation profile obtained by earlier workers [5, 6] and agrees with the results Kantz [1] obtained using polypropylene (a highly oriented skin, a shear nucleated spherulitic intermediate layer and a spherulitic core).

Crystallinity effects have been shown to change the mechanical properties and the mode of fracture of a semi-crystalline polymer, nylon 6, from brittle to ductile [10]. Similarly, in nylon and polypropylene it has been shown that there is a marked increase in yield stress and shear modulus with crystallinity [11]. Both pressure and shear stress are known to alter the crystallization process drastically and Keller and Machin have shown that the level of stress in a melt during crystallisation influences the induced morphology [12]. This would appear to indicate that a variation of degree of crystallinity across an injection-moulded bar could be expected.

The work reported here is part of an overall programme to study the effect of various amounts of short fibre reinforcement on the morphology, microstructure, fracture behaviour [13, 14] and ultimate strength properties of injection moulded semi-crystalline thermoplastics. The correlation of mechanical property and fracture behaviour in such materials is limited and the objective of this initial work is to identify the particular morphological and crystallization variable or variables which govern the ultimate tensile properties and fracture behaviour of the unfilled matrix polymer under normal moulding conditions. Also, these structural variations are related to the rheological process involved and an attempt is made to relate Tadmor's model for complex orientation effects in amorphous thermoplastics to the semi-crystalline material studied here.

2. Experimental

2.1. Specimen preparation

Tensile bars to ASTM standard D638-68 type I were moulded in PTMT grade TAP 10 by Pilkington Brothers Ltd using an Anker A 17.65 injection moulder. A mean barrel temperature between 230 and 240° C, a mould temperature of 40° C, an injection pressure of 950 psi and a total cycle time of 51 sec were used for all samples. Particular care was taken to obtain reproducible void-free specimens.

2.2. Etching studies

Specimens were cut from the ASTM tensile bars perpendicular (section A) and parallel (sections B and C) to the injection direction as shown in Fig. 1.

Section A was polished to 600 μm using emery paper and then to 0.25 μm using diamond paste wheels. The polished surface was examined under the optical microscope to ensure it was free from gross scratches (1 to 2 μm). Solvent etching was carried out, using concentrated o-chlorophenol, to reveal the morphology of the section which was then studied using optical and scanning electron microscopy. As a result of the features revealed in section A, section B was further sectioned taking three layers across the width of the bar (Fig. 1) to correspond to the different regions indicated in section A. Section C was similarly layered, but in

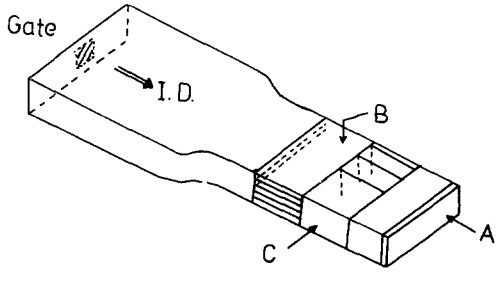

Figure 1 Diagram of an injection-moulded tensile bar indicating the sections taken for etching, microtomy and diffractometry studies. The arrows are directed perpendicular to the face of each section taken.

this case across the thickness of the bar. Polishing and etching of all these sections was carried out in an identical manner to that used for section A.

2.3. Microtome studies

Sections for microtoming were cut using a jeweller's saw to reveal identical faces to those used in the etching studies (Fig. 1) and sledge microtome sections were taken using a Leitz microtome. Thinner sections obtained using an L.K.B. ultra microtome were floated from water on to a glass slide; these were viewed with polarized light to enable spherulite size measurements to be taken.

2.4. X-ray studies

X-ray diffraction patterns were obtained using a Philips X-ray machine and Cu$K\alpha$ radiation. Specimens were cut initially so that diffraction patterns from three directions, 90° apart, could be obtained in order to identify any orientation present. Further specimens were cut, using a diamond wafering blade, as in C (Fig. 1) to give sections of the different regions. The much thinner surface layer was removed by sledge microtomy. Specimen thickness was otherwise between 500 and 600 μm. Similar specimens were taken in the B section (Fig. 1).

For quantitative analysis of peak intensity and crystallinity a McLean X-ray diffractometer was used. The previous specimens were studied using this apparatus and in order to gain an indication of reproducibility identically positioned specimens were taken from the A.S.T.M. bars and similarly tested. A completely amorphous specimen, obtained by extrusion through a slit die and then chilling on water rolls to give a cast film, when similarly tested gave results showing the contribution possible due to the amorphous content of the polymer. A computer program was written so that the data, obtained from the X-ray diffractometer on computer tape in terms of intensity and the Bragg angle, could be fed into a computer which standardised the results, compared the main peak intensities, calculated the proportional crystallinities and finally plotted a crystallinity profile of the bar.

2.5 Microhardness studies

Microhardness testing of a polymer carried out by measuring the lengths of a dimaond indentation includes a relaxation factor which must be considered when comparing hardness values of these materials.

Sections parallel and perpendicular to the injection direction were cut from an Â.S.T.M. bar and polished to 600 μm using emergy paper and to 6 μm using diamond paste. The sections were then coated with gold–palladium to aid focussing during microhardness testing. Measuring the length of the diamond indentation proved difficult but a series of measurements provided confirmation of features present in the microhardness profile of the width of the bar. These results could not, on their own, be considered sufficiently accurate but they did give a meaningful correlation with spherulite size and crystallinity.

2.6. Fracture studies and microscope examination

Tensile bars in the as-moulded condition were strained to fracture on an Instron tensile testing machine at a strain-rate of 0.2 cm min^{-1} to obtain values of tensile strength, elongation to break,

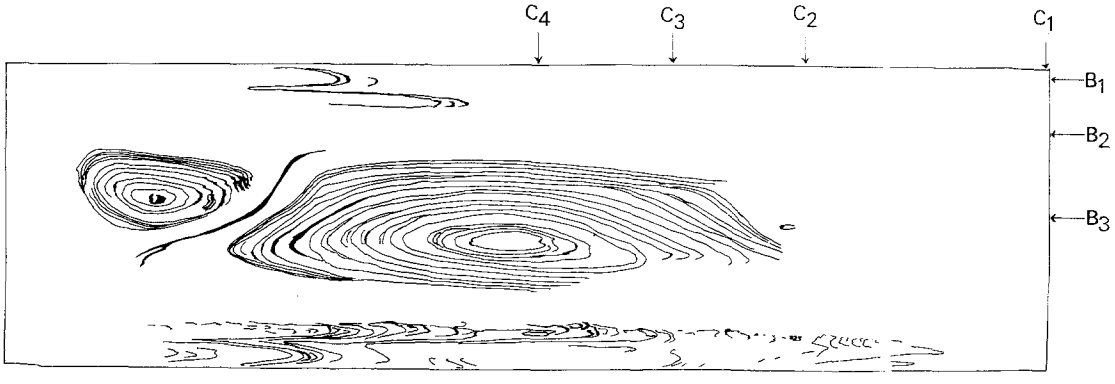

Figure 2 Schematic representation of the flow lines revealed in section A by mocrotomy and etching studies. Also indicated are the positions at which the sections B and C were taken.

elongation to neck, modulus of elasticity or offset yield strength and maximum load. Also, a number of samples were strained over a range of extension values and sections from these tensile bars were taken parallel and perpendicular to the injection direction and etched or microtomed prior to micro-photographic study using a Reichert polarization microscope or a Cambridge stereoscan scanning electron microscope.

3. Results and discussion

3.1. Morphology and microstructure

All sections taken as shown schematically in Fig. 1 revealed a gradual change in morphology across the specimen as the distance from the skin increased; this can be accounted for by the three-dimensional cooling effects that take place in the mould. For this reason it was not possible to find a region of reasonable size containing an unchanging microstructure and in the following discussion each section will be considered in turn with respect to its position in the specimen. Fig. 1 shows schematically part of an end-gated tensile bar and indicates the positions from which sections were taken; section A was taken perpendicular to the injection direction and viewed parallel to this direction as indicated by the arrow; B was taken parallel to the injection direction and viewed along the arrow direction and similarly C.

Within each section shown in Fig. 1 the layers were numbered; A_1 for the single layer of A, layers in B were labelled for the surface, B_1 denoting the top layer, B_2 the layer beneath and B_3 the layer through the centre of the bar thickness; section C was similarly labelled beginning with C_1 at the edge and continuing with C_2, C_3 and C_4 to the centre of the bar, this time progressing across the bar's width.

Fig. 2 is a plan of section A_1, perpendicular to the injection direction and shows schematically the flow lines revealed in this direction and also the relative positions of B_1, B_2, B_3 and C_1, C_2, C_3 and C_4 with respect to the section. The arrows on the figure represent the direction in which B_1, B_2, B_3, C_1, C_2, C_3 and C_4 were taken through the bar.

The morphology of section A_1 is clearly revealed in the microtomed section shown in Fig. 3 which is an optical micrograph of an area of A_1. As well as indicating the positions of B_1, B_2 and B_3 (as in Fig. 2) it shows that the borderline between the bands generally recognized as skin, transition and core is diffuse. In this specimen four bands can be identified, extending to the centre of the bar. The non-spherulitic layer on the surface of

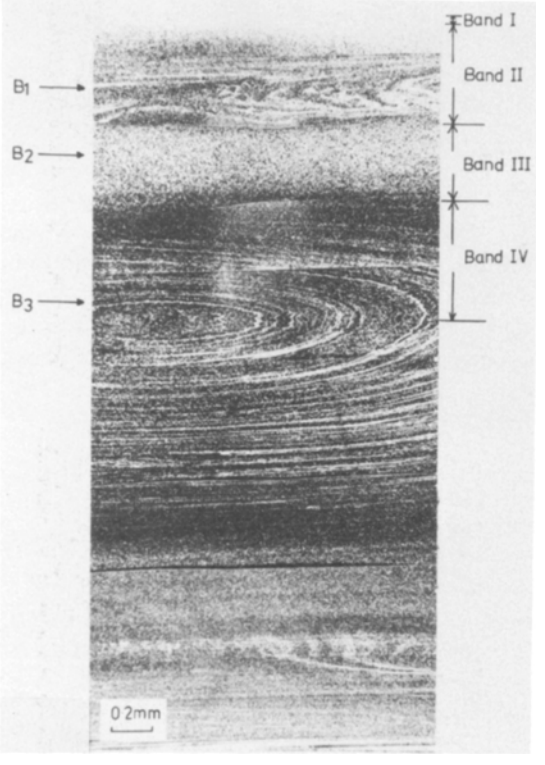

Figure 3 An optical micrograph taken across the width of the microtomed section A, indicating the four bands and the positions at which the sections B were taken.

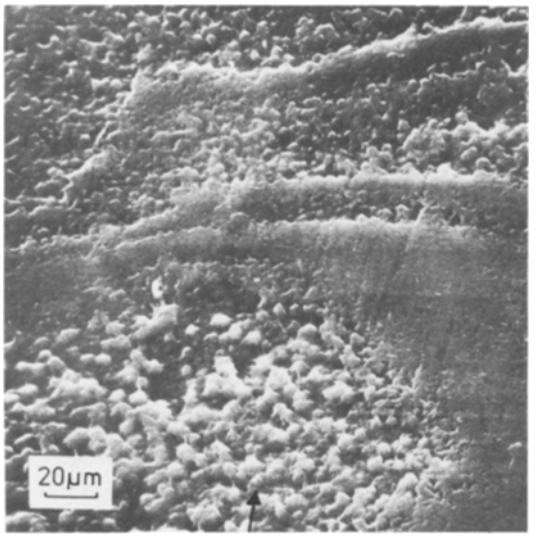

Figure 4 Scanning electron micrograph of the etched section B_1 showing the two component flow pattern structure. The arrow indicates the more vigorously attacked area outside the flow line.

the specimen is referred to as band I, the adjacent band containing flow lines as band II and successive bands as III and IV. Another four bands can be identified for completeness, but these would be similar to those indicated, the bar being symmetrical about its centre.

The microtomed section B_1, taken just below the surface layer revealed the flow lines previously indicated in section A_1 from Fig. 3. Under higher magnification the microtomed sections reveal two types of micro-structures within the flow pattern region, one consisting of spherulites of similar size and form to those in band III and the other consisting of smaller spherulites which form the actual flow line. Micrographs of etched sections from the flow pattern region, taken using the scanning electron microscope show a corresponding two component structure. Fig. 4 shows part of the etched region, outside the flow line, (indicated by the arrow) to have a nodular appearance consisting of structures approximately 2 μm diameter. Thin microtomed sections of this area, immediately below the surface layer reveal spherulites of similar size. Since the etchant works by removal of amorphous material the flow pattern suggests regions of varying amorphous content i.e. differing crystallinity. The relative degree of crystallinity within the flow lines depended upon their position in the bar. Those flow lines in band II etched less efficiently than the surrounding area indicating that the flow lines cause an increase in the overall crystallinity of that region, whereas those flow lines in band IV were found to etch more efficiently than the immediate surrounding area. The flow lines were too small for their percentage crystallinity to be determined, however section A_1 (Fig. 3) revealed a layer structure consisting of four different bands, (1) non-spherulitic, (2) loosely-packed flow lines, (3) a region without visible flow lines, (4) tightly packed flow lines. With these observations in mind it is apparent that the changes in crystallinity on the larger scale should give information concerning variations on the microscale. Section B_2, in Fig. 3, taken through band II is distinguished by its lack of flow pattern. With increasing distance from the edge of the specimen there is more resistance to attack by the solvent etch, indicative of an increase in

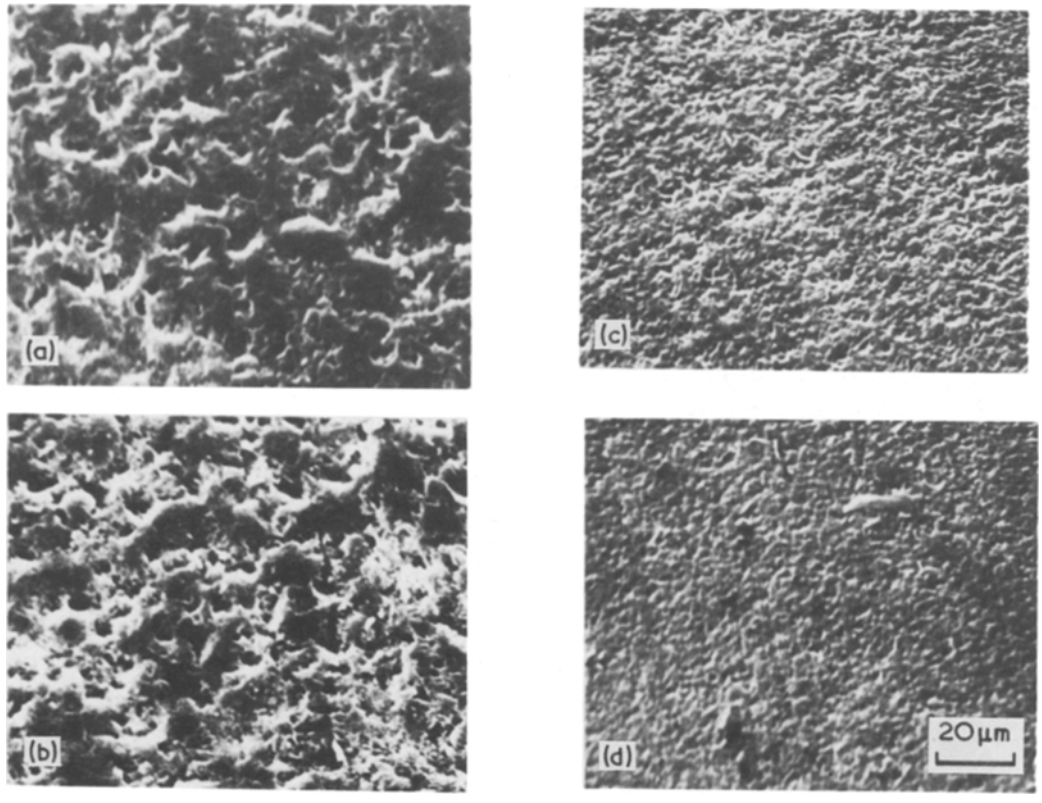

Figure 5 (a) to (d) Series of scanning electron micrographs of the etched section B_2 showing decreasing susceptibility to attack towards the centre of the tensile bar and the lack of flow lines.

crystallinity towards the centre. Fig. 5a to d shows the lack of flow pattern and the decrease in susceptibility to etch with distance from the specimen edge. Fig. 5a was taken from the edge of the specimen and shows vigorous attack by the etchant has destroyed part of the structure, Fig. 5b was taken a little further within the specimen, Fig. 5c shows the less efficiently etched region nearer the centre and Fig. 5d was taken at the centre of the bar where the etchant revealed little of the microstructural features.

Section B_3 taken through band III (Fig. 3) showed features similar to C_4 which can be seen in more detail in Fig. 6.

Etching of section C_1 destroyed any recognizable structure, the solvent etch preferentially attacking disordered regions; microtome sections showed a birefringent but non-spherulitic layer.

Section C_2 was taken at a position one quarter through the bar and the microstructure of this section was almost homogeneous, with only a gradual change from surface layer to centre which, considering its position (Fig. 2) is to be expected.

Section C_3 (Fig. 2) revealed the beginning of flow at the centre. When the section was etched the nodule size outside of the flow lines increased to a maximum near the outside edge of band III and then decreased. The nodular appearance was difficult to distinguish near the centre of the specimen as the resistance of the material to the etchant increased.

Section C_4 (Fig. 2) taken through the centre of the bar reveals the detailed flow lines shown in Fig. 6 with those in the centre in the injection direction and those in band II in the opposite direction.

The flow lines at the centre of the mould were unexpected but, under the moulding conditions used, it is likely that even the central region was beginning to solidify during filling of the mould. The increased viscosity, creating shear stresses, would cause variation in crystallinity and the flow lines would then represent contours of crystallinity.

Measurements from sections parallel to the injection direction of bands I to IV showed that the non spherulitic layer (band I) varied in depth

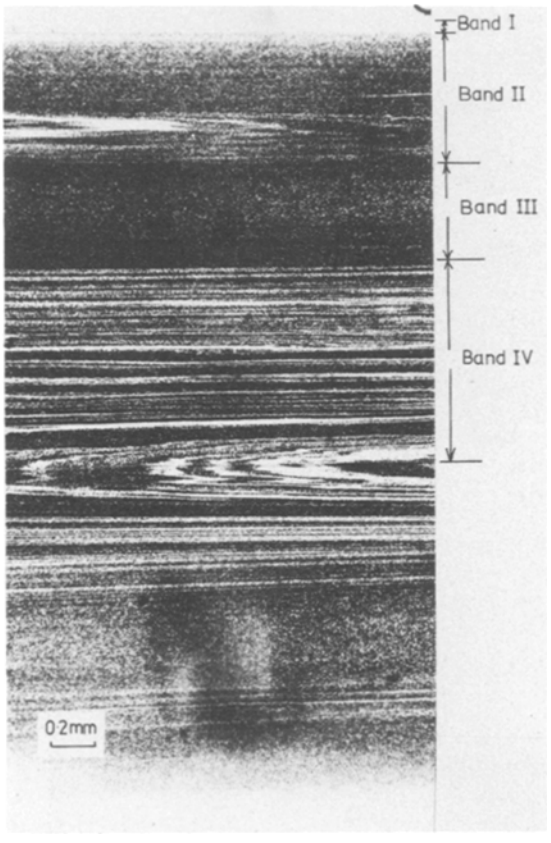

Figure 6 Optical micrograph of the microtomed section C_4 revealing the band structure and the opposing directions of the flow lines in bands II and IV.

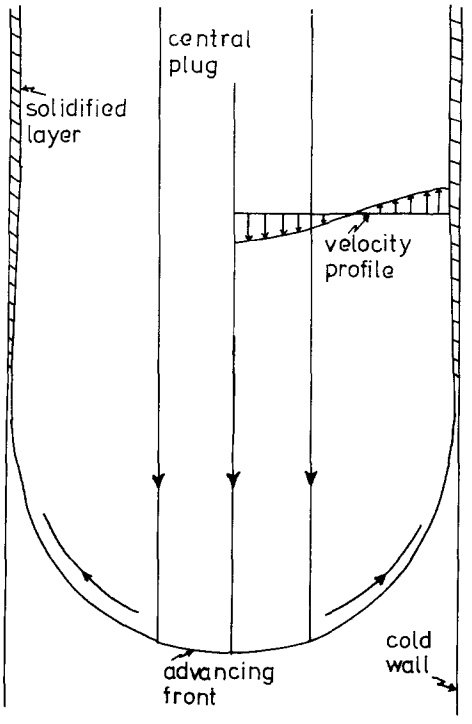

Figure 7 Diagram representing a modification of Tadmor's model for mould filling incorporated plug flow in the central region.

between 20 and 50 μm and that bands II, III and IV had remained almost unchanged in widths in all specimens. Band II was approximately 550 μm, band III approx. 450 μm and band IV approx. 625 μm. The spherulite size varied with increasing distance from band I to band IV and ranged from 2 to 7 μm.

The results of these sectioning studies reveal the presence of four bands, two of which contain flow lines and indicate movement in opoosing directions; this suggests that the mould filling may be partially represented by a modification of Tadmor's model incorporating "plug flow" in the central region. A suitable modification of the model is illustrated in Fig. 7. The polymer enters the mould and reaches the advancing front as a "plug" of material, elongational flow is induced and solidification of the fluid particles occurs as they meet the cold wall, freezing in the orientation. Relaxation of orientation within the solidified layers occurs after cessation of flow, the time for relaxation depending upon the distance from the mould surface. At this stage of modification the model implies that some orientation should be present in the injection moulded bar.

The difference between this four-band morphology and that obtained by other workers [2] is possibly due to a combination of barrel temperature and injection speed. Investigation of these factors was outside the scope of the work undertaken but it does indicate the need for complete instrumentation of the injection moulder when working with this material.

3.2. Orientation and crystallinity studies

The Debye patterns obtained using the Philips X-ray machine showed no orientation in any of the undrawn sections as shown in Fig. 8. A standard specimen, obtained by melting PTMT granules at 230° C and then cooling rapidly in air before degrading became significant, gave an identical pattern.

The computer program, designed to analyse the sets of results, received values of θ, the Bragg angle and I, the intensity of X-rays diffracted from the plane, defined by the Bragg angle, from the McLean X-ray diffractometer. A typical graph of these data is given in Fig. 9. The sections studied were not all of identical thickness and standardization of results was required to remove this factor. Peaks were obtained using Cu $K\alpha$ radiation

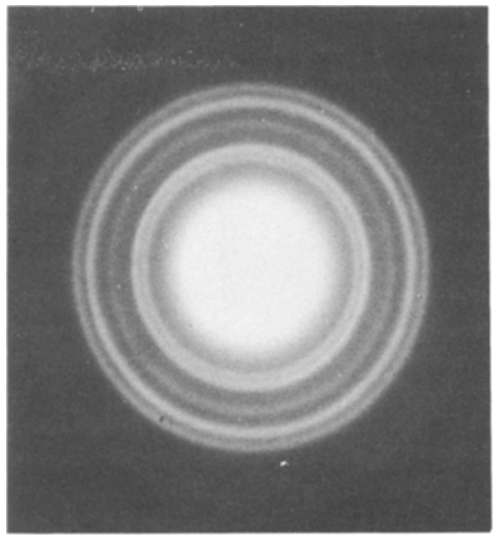

Figure 8 Typical Debye pattern of undrawn PTMT; no orientation was observed in any of the bands.

when θ was between 8 and 18°. The intensity of diffracted X-rays tended to increase towards the low angle values due to the influence of the main beam and so, for standardization purposes, the values at the 18° end of the graph were taken where the intensity was at a minimum for all values of θ greater than this. The computer, in standardizing all the graphs, took five values about the angle of 18° for each graph, averaged then and set them to one particular value. All intensity values were altered to correspond with the adjustment required. The background intensity was removed by calculation of the straight-line function between the two points $\theta = 8°$ and 18°, subtaction of the area beneath this line creating a new horizontal axis.

The modified amorphous specimen graph was fitted to the crystalline specimen graphs by an iterative computer routine by which the amorphous intensity values were doubled to ensure that they were all greater than the crystalline intensity values and then the amorphous curve wad reduced until the distance where the graphs lay furthest apart becoma zero. The area between the two curves was then considered to be proportional to the crystallinity. The removal of the amorphous intensity was carried out on every set of values and the complete set plotted out as shown in Fig. 10. By plotting the crystallinity values obtained against the position of the specimen in the tensile bar a crystallinity profile was obtained. For a bar allowed to cool without any of

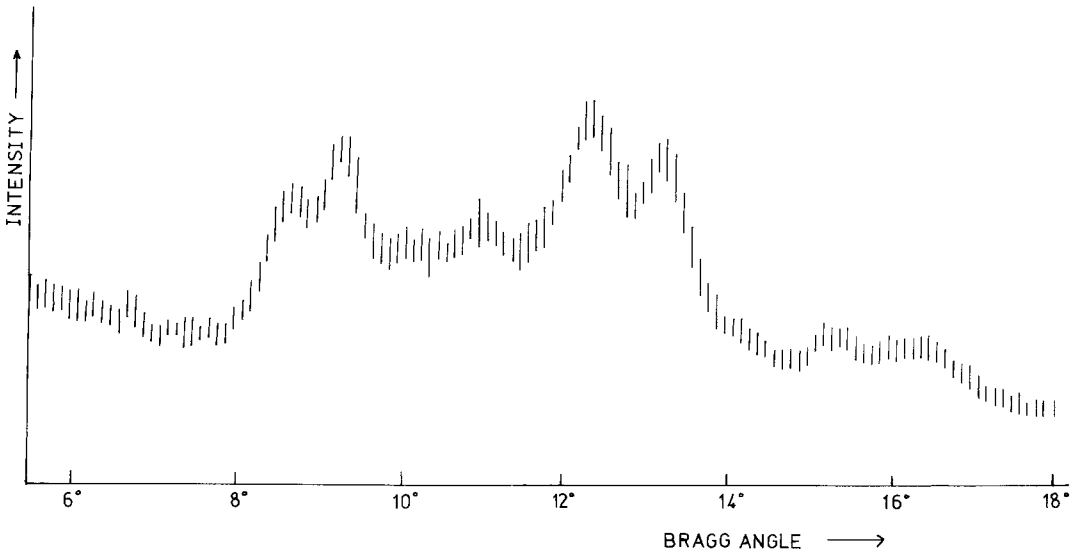

Figure 9 Graph obtained from the McLean diffractometer before standardisation showing the intensity of the diffracted beam as a function of the Bragg angle.

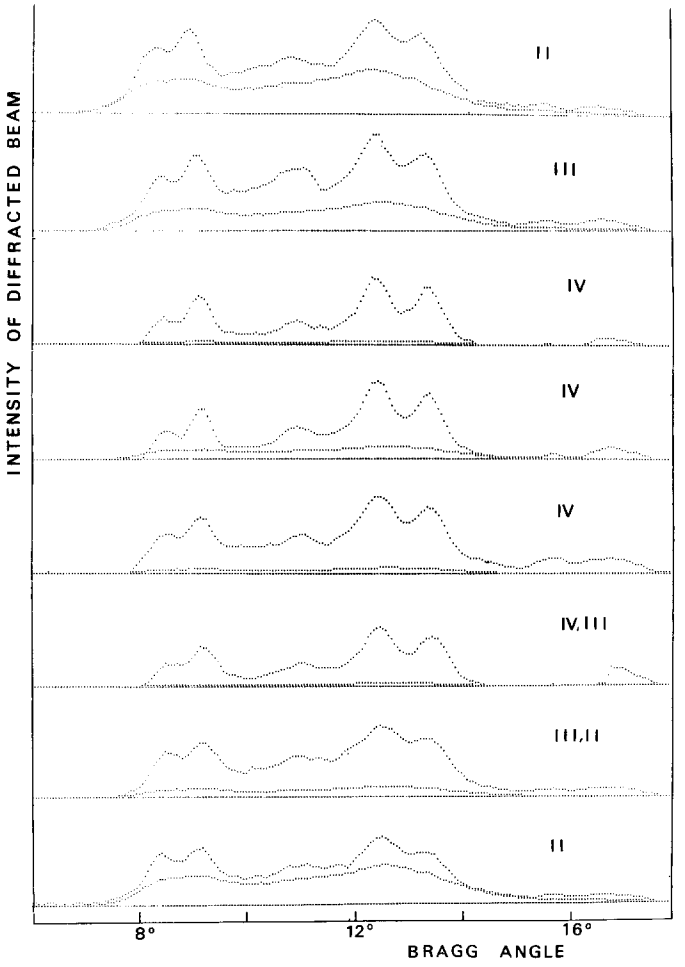

Figure 10 Modified X-ray diffraction curves showing the variation of crystallinity across the injection-moulded bar.

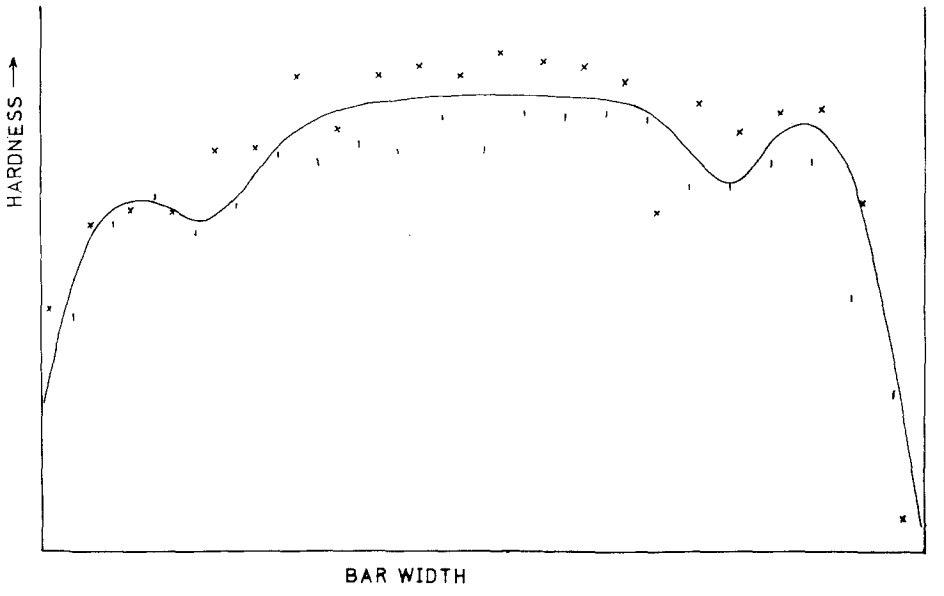

Figure 11 Microhardness plot of the cross-section of a tensile bar showing an increase towards the centre but also revealing two possible regions of lower hardness. Two sets of data are shown but other series measured showed a similar trend.

the shear stress effects due to flow. The crystallinity profile would be expected to give a maxima near the centre of the specimen. However, that from the injection-moulded specimen rises in band III but falls to a near constant value across the centre of the bar before symmetrically increasing in band III and then decreasing towards the edge of the specimen.

The microhardness profile as shown in Fig. 11, shows a general increase towards the centre of the

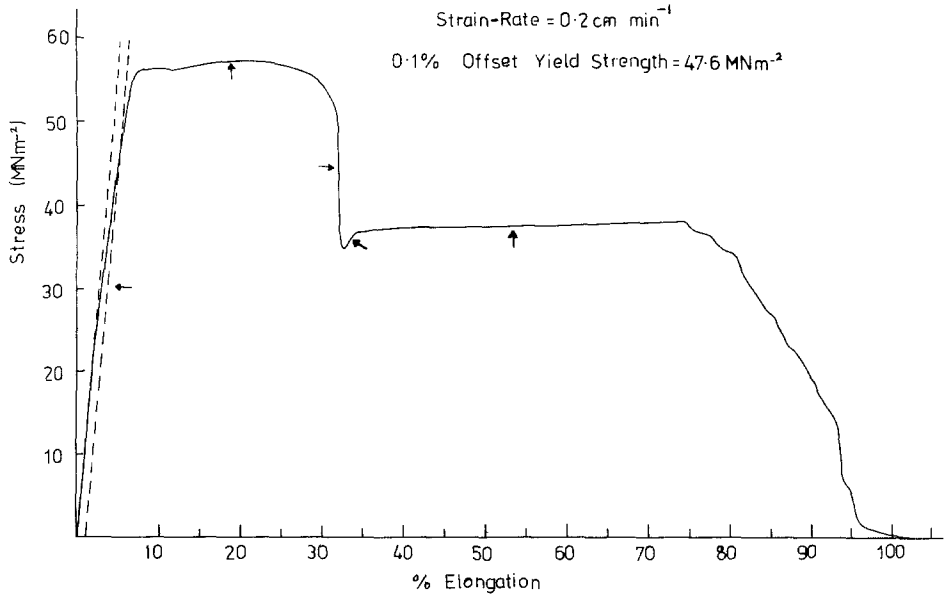

Figure 12 The stress versus elongation curve typical of unfilled PTMT revealing the four stages of deformation before ultimate failure. The arrows indicate the positions at which the fracture cycle was halted in order to study the deformation at these elongations.

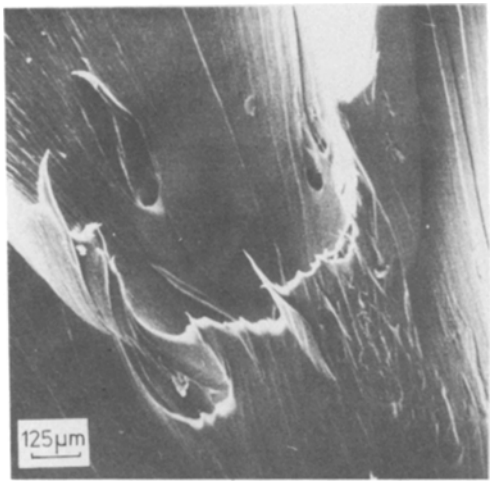

Figure 13 Scanning electron micrograph of part of the fracture surface showing the variation in void size caused through deformation.

bar but with a possible decrease in band III corresponding to the region of larger spherulites and higher overall crystallinity.

3.3. Fracture behaviour

Fracture occurred by necking, drawing and then subsequent failure of the specimen and took place at the minimum cross-sectional area of the bar, approximately 2 cm off-centre and away from the gated end. A ductile fracture occurred with percentage elongations ranging between 60 and 102%. The percentage elongation at which necking commenced was, in all samples, almost identical at 32.4% and maximum elongation occurred when the initial neck was formed at 90° to the tensile direction. Fig. 12 shows the stress versus elongation curve obtained indicating four regions: (1) uniform deformation, (2) yield without necking at a stress of $57\,MN\,m^{-2}$, (3) yield by necking at a stress of $37\,MN\,m^{-2}$ but with a considerably diminished cross-sectional area, (4) slow fracture with continued elongation and decreasing stress load.

In all cases, voids with considerable size variation were observed on the fracture surface, as can be seen in Fig. 13, and can be considered as potential regions for sink and cavity formation. Fracture was initiated by formation of a sink in the necked region, usually approximately one third of the bar width in from the edge, and continued by extension of the void to the surface creating a cavity. A micrograph of this, obtained by stopping the Instrom machine before the fracture cycle was complete, is shown in Fig. 14. Failure then occurred by tearing of the specimen from this cavity or, alternatively, by creation of other cavities which finally coalesced across the width of the specimen causing complete separation to occur. Elongation during the process of cavity extension was significant and gave markedly fibrillar fracture surface which could be divided into two distinct regions, an inner and an outer zone. The outer zone consisted of very long fibrils fractically unbroken in thier drawing as shown in Fig. 15a. The inner zone, in contrast, consisted of shorter fibrils (Fig. 15b).

Fig. 12 indicates those positions where the fracture cycle was stopped to obtain specimens of varying deformation. All specimens were etched prior to examination; however, this was not possible with those sections perpendicular to the stress direction once necking had begun; these were microtomed. Etching revealed little change in the microstructure until necking began; at this stage band IV etched similarly to band II but in neither case did the etching show any visible spherulitic deformation. Sledge microtome sections of the complete cross-section of the neck, taken perpendicular to the tensile direction, when viewed by low power optical microscopy revealed a whitened oval inner zone. Viewing through crossed Nicols revealed no marked difference to the unstrained sample apart from the presence of stress birefringence. However, ultra microtomed sections of the inner and outer zones did reveal a

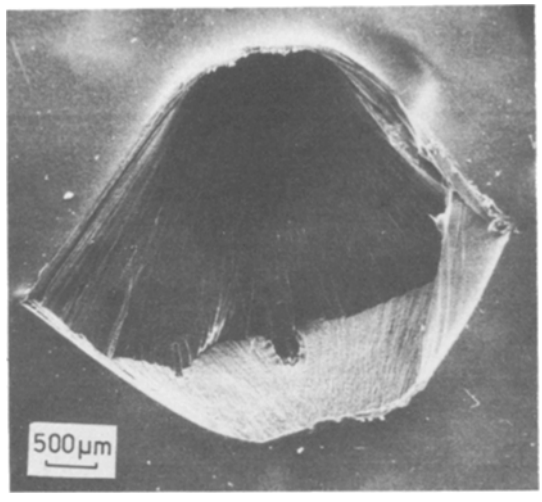

Figure 14 Scanning electron micrograph of a cavity on the surface of a deformed specimen.

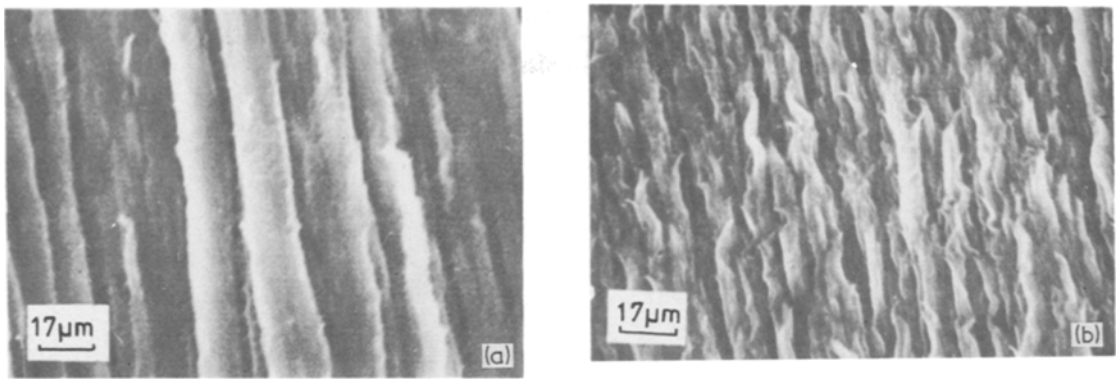

Figure 15 Scanning electron micrographs of (a) the outer region of the fracture surface showing the long practically unbroken fibrils, (b) the central region of the fracture surface revealing shorter fibrils.

difference; in the unstrained sample spherulites were clearly visible but in the necked samples the spherulites were only barely recognizable. Two micron sections taken parallel to the injection direction of the necked region revealed two distinct types of microstructure which can be seen in Fig. 16. The whitened inner zone seemed completely spherulitic with spherulites approximately 3 μm diameter but in the outer zone slightly larger spherulites were separated by birefringent but non-spherulitic regions. The inner zone corresponded in width to band IV, the outer zone corresponding to bands I, II and III. With increased extension of the necked sample the flow lines in the inner zone became more tightly packed until finally they could barely be distinguished. Otherwise, sectioning of the drawn bars indicated gradual deformation of the two zones with increased extension but with the deformation of the outer zone being far more distinctive than within the inner zone.

Debye patterns of the un-necked region of the fracture specimen showed little orientation which suggests that during this stage of deformation (Fig. 12) the polymer chains are unravelling but have not lined up to any extent. When the majority are fully unravelled a second stage of deformation takes place in which the chains in the outer zone become more and more extended, the spherulites becoming unrecognizable, whereas the deformation in the inner zone although consisting of some spherulitic extension, also includes recrystallization which enables large numbers of spherulites to be distinguished after fracture has occurred. However, within the inner zone there are also regions of deformation identical to that in the outer zone, these correspond to the areas outside of the flow lines which were previously noted to have a similar spherulitic appearance to those in band III. The microhardness profile of the bar after necking shows a minimum at the centre of the bar corresponding to the region of recrystallization.

4. Conclusions

The morphology of an ASTM bar of PTMT has been shown to consist of four bands, two of which are distinguished by the presence of flow lines containing spherulites smaller than the surrounding areas. A modification of Tadmor's model has been shown to adequately represent the mould filling, with the incorporation of plug flow and a modification of the elongation flow describing the solidification of a completely isotropic surface layer and intermediate zone (band III), the latter containing none of the shear nucleated spherulites suggested by the original model at this position of maximum shear. The crystallinity profile indicates an increase in crystallinity in the nonflow regions whereas the microhardness profile indicates a decrease in hardness in this region, which contains an overall majority of larger spherulites.

The fracture behaviour can be considered in terms of the band structure; band IV with its comparably lower crystallinity but maximum overall hardness consists mainly of the smaller spherulites, contained within tightly packed flow lines, which play the major role in deformation during necking, through recrystallization. In the other bands where the flow lines play a less important role, the deformation of these slightly softer, but more crystalline regions containing a

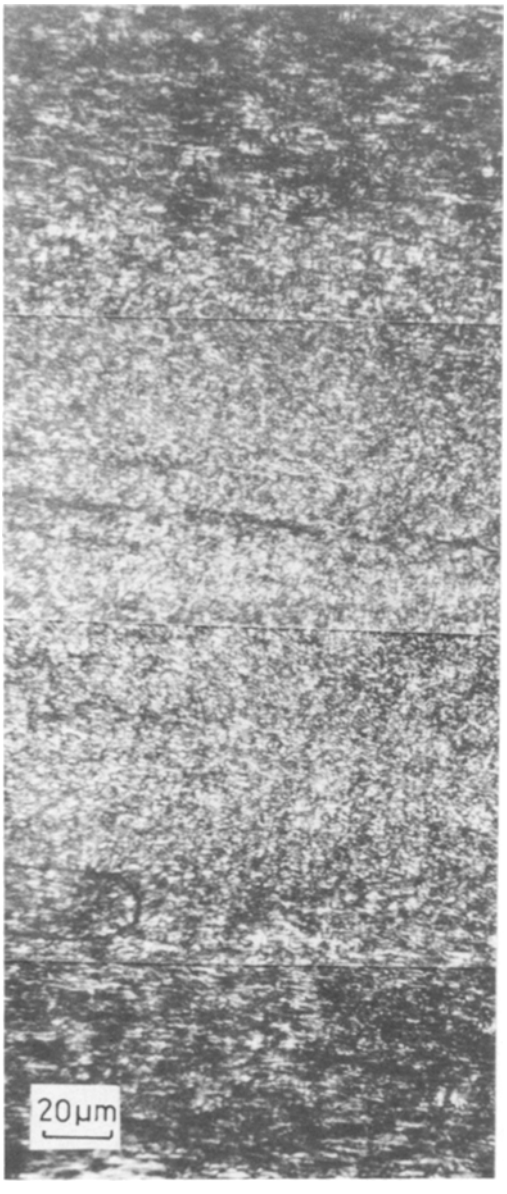

Figure 16 Optical micrograph of an ultra microtomed section of a fractured specimen taken perpendicular to the tensile direction. Two zones are clearly distinguished.

majority of larger spherulites is by drawing of the spherulite to unrecognizable limits. However, neither deformation is completely limited by the zone dimensions, recrystallization, as indicated by the presence of flow lines, occurring in the outer zone and extensive spherulite drawing occurring within the inner zone.

Acknowledgement

The authors wish to acknowledge the award of an S.R.C. research studentship (J.C.)

References

1. M. R. KANTZ, *Int. J. Polymer Mater.* 3 (1974) 245.
2. S. Y. HOBBS and C. F. PRATT, *J. Appl. Polymer Sci.* **19** (1975) 1701.
3. T. W. OWEN and D. HULL, *Plastics and Polymers* **42** (157) (February 1974) 19.
4. J. BOWMAN, N. HARRIS and M. BEVIS, *J. Mater. Sci.* **10** (1975) 63.
5. G. MENGES and G. WÜBKEN, 31st Annual Technical Conference of Society of Plastics Engineers (SPE ANTEC) Montreal, Canada, Vol. 19 (1973) pp. 519–22.
6. R. L. BALLMAN and H. L. TOOR, *Mod. Plastics* 38 (October 1960) 113.
7. Z. TADMOR, *J. Appl. Polymer Sci.* **18** (1974) 1753.
8. H. R. KANTZ, H. D. NEWMAN, JUN and F. H. STIGALE, *ibid* **16** (1972) 1249.
9. E. S. CLARKE, *Appl. Polymer Symp.* **24** (1974) 45.
10. T. J. BESSELL, D. HULL and J. B. SHORTALL, *J. Mater. Sci.* **10** (1975) 1127.
11. H. W. STOURWEATHER and R. E. BROOKS, *J. Appl. Polymer Sci.* **1** (1959) 236.
12. A. KELLER and M. J. MACHIN, *J. Macromol. Sci. (Phys) B* (1967) 41.
13. P. F. VINCENT, *Polymer* **1** (1960) 7.
14. A. PETERLIN, "The Solid State of Polymers" (Marcel Dekker, New York, 1974) p. 83.

Received 12 March and accepted 26 May 1976.